Modulation of Nanotube Formation by Structural Modifications of Sphingolipids

Vitthal S. Kulkarni,* Joan M. Boggs,# and Rhoderick E. Brown*

*The Hormel Institute, University of Minnesota, Austin, Minnesota 55912 USA, and #Department of Biochemistry, Hospital for Sick Children, University of Toronto, Toronto, Ontario M5G 1X8, Canada

ABSTRACT Galactosylceramides (GalCers) containing nervonoyl (24:1$^{\Delta 15(cis)}$) acyl chains have the capacity to assemble into nanotubular microstructures in excess water (Kulkarni et al., 1995. *Biophys. J.* 69:1976–1986). To define the structural parameters that modulate nanotube formation, GalCer derivatives were synthesized that contained *cis* monounsaturated acyl chains with the formula X:1$^{(X-9)}$. X indicates the total acyl carbon number (24, 22, 20, or 18), and 1 indicates a single *cis* double bond, the location of which is designated by the superscript (X-9). Deep etching of freeze-fractured 24:1$^{\Delta 15(cis)}$ GalCer dispersions followed by replica production and transmission electron microscopic analysis confirmed nanotube morphology (25–30-nm diameter). Control experiments revealed that tubule formation was promoted by cooling through the main enthalpic phase transition coupled with repetitive freeze-thaw cycling. Imparting a negative charge to the sugar headgroup of 24:1$^{\Delta 15}$GalCer via sulfate dramatically altered mesomorpholgy and resulted in myelinic-like, multilamellar structures. Removal of the sugar headgroup (24:1$^{\Delta 15}$Cer) resulted in flattened cylindrical structures with a cochleate appearance. Compared to these large-scale changes in morphology, more subtle changes were induced by structural changes in the acyl chain of 24:1$^{\Delta 15}$GalCer. 22:1$^{\Delta 13}$GalCer dispersions consisted of long, smooth tubules (35–40-nm diameters) with a strong tendency to self-align into bundle-like aggregates. In contrast, the microstructures formed by 20:1$^{\Delta 11}$GalCer resembled helical ribbons with a right-handed twist. Ribbon widths averaged 30–35 nm, with helical pitches of 80–90 nm. 18:1$^{\Delta 9}$GalCer displayed a variety of morphologies, including large-diameter multilamellar cylinders and liposome-like structures, as well as stacked, plate-like arrays. The results are discussed within the context of current theories of lipid tubule formation.

INTRODUCTION

Nonliposomal lipid assemblies have received increasing attention in recent years because of their usefulness as organizational templates in crystallization, metallization, and mineralization processes (Schnur, 1993; Archibald and Mann, 1993), as well as their potential advantages as drug delivery vehicles. Lipid monolayer assemblies have been used to achieve two-dimensional crystallization of certain proteins for which insufficient quantities and/or other problems prevent three-dimensional crystallization from solution (e.g., Chiu et al., 1997; Kulkarni et al., 1995c). Moreover, cylindrical glycolipid nanotubes provide helically symmetrical scaffolds that can promote two-dimensional helical crystallization of proteins and thus obviate the need for tilt series reconstruction during image analysis (Wilson-Kubalek et al., 1998; Darst, 1998). In biomedical applications involving drug delivery, nonliposomal assemblies produced from naturally occurring amphiphiles may provide more suitable means to achieve a controlled and sustained release of certain dissolved or entrapped drugs (Goldstein et al., 1997). Thus investigations into the physiochemical parameters governing amphiphile assembly continue to spark important new technological developments.

Among naturally occurring lipid species that assemble into cochleate cylinders, nanotubes, and fiber-like microstructures, sphingolipids such as galactosylceramides and related derivatives have attracted attention recently (Archibald and Yager, 1992; Archibald and Mann, 1993, 1994; Kulkarni et al., 1995a,b, 1996; Goldstein et al., 1997). Galactosylceramides and their sulfated relatives, i.e., sulfatides, are normally enriched in myelin sheath, intestinal, and kidney brush border membranes. These simple sphingolipids are thought to provide structural stability to membranes by way of their strong intermolecular interactions and, in doing so, to impart and maintain the curvature and cylindrical shape of certain membranes (Curatolo and Neuringer, 1986; Maggio et al., 1988). The tendency of naturally occurring galactosylceramides to form helical ribbon-like structures was originally noted within the cells of patients afflicted with globoid cell leukodystrophy (Yunis and Lee, 1970). In subsequent studies in which nonaqueous solvents were used to promote self-assembly (Archibald and Yager, 1992; Archibald and Mann, 1993, 1994), bovine brain GalCer and its subfractions assembled into cochleate cylindrical structures and related high axial ratio microstructures. Recent investigations into the self-assembly of individual molecular species of GalCers have established that certain manipulations of the acyl or headgroup structure play major roles in modulating whether cylindrical microstructures form at all, as well as determining what features the high axial ratio microstructures display. For instance,

Received for publication 25 November 1998 and in final form 13 April 1999.

Address reprint requests to Dr. Rhoderick E. Brown, Hormel Institute, University of Minnesota, 801 16th Avenue NE, Austin, MN 55912-3698. Tel.: 507-433-8804; Fax: (507)437-9606; E-mail: reb@maroon.tc.umn.edu.

Dr. Kulkarni's present address is The Collaborative Group, 3 Technology Drive, East Setauket, NY 11733-4072.

0006-3495/99/07/319/12 $2.00

introducing one *cis* double bond at carbon 15 of the 24-carbon acyl chain ($24{:}1^{\Delta 15}$) of GalCer results in nanotube-like structures rather than ribbon-like structures being formed when GalCer is cyclically heat treated and freeze-thawed under aqueous conditions (Kulkarni et al., 1995a,b). Nanotube formation of 24:1 GalCer assemblies also results when the glycolipid is precipitated from dimethylformamide/water (Goldstein et al., 1997). Changes to headgroup structure influence the morphology of 24:1 glycolipid assemblies. Although replacement of the galactose headgroup with glucose still results in needle-like and fiber-like microstructures upon hydration (Mutz et al., 1990), substitution with phosphorylcholine or proline prevents formation of discrete high axial ratio microstructures (Kulkarni et al., 1995a; Goldstein et al., 1997). Yet, completely removing the galactose headgroup does not prevent formation of high axial ratio microstructures, although they appear solid and cochleate rather than tubular (Goldstein et al., 1997).

To provide a better understanding of the physicochemical parameters responsible for establishing the delicate balance of intermolecular forces that control molecular packing and self-assembly in high axial ratio microstructures, we examined the effect of *cis* monounsaturation in the acyl region of GalCer as well as the effect of polar headgroup modifications on lipid mesomorphology by electron microscopic approaches. To accomplish this goal, several GalCer derivatives were synthesized and purified that contained homogeneous acyl chains of differing length and with differing *cis* double bond location. Aside from relying solely on freeze-fracture electron microscopic approaches to characterize the lipid assemblies, deep-etching techniques were utilized to enhance structural details. The effects of different experimental conditions on nanotube formation of 24:1 GalCer also were characterized.

MATERIALS AND METHODS

Synthesis of GalCer derivatives with homogeneous acyl chains

Fatty acids were purchased from Nuchek Prep. (Elysian, MN). Other reagents were obtained from Sigma-Aldrich. *N*-Acylated galactosylsphingosines with homogeneous fatty acyl residues consisting of *cis*-15-tetracosenoate ($24{:}1^{\Delta 15}$), *cis*-13-docosenoate ($22{:}1^{\Delta 13}$), *cis*-11-eicosenoate ($20{:}1^{\Delta 11}$), *cis*-9-octadecenoate ($18{:}1^{\Delta 9}$), or *cis*-9,12-octadecenoate ($18{:}2^{\Delta 9,\ 12}$) residues were synthesized and purified as described previously (Kulkarni et al., 1995a; Smaby et al., 1996). In the notation ($X{:}Y^{\Delta z}$), X indicates the total number of carbons and Y indicates the total number of *cis* double bonds located at the carbon(s) positions designated by the superscript (Δz). Briefly, the *N*-hydroxysuccinimide ester of the desired fatty acid was prepared, recrystallized, and reacted with psychosine (lyso-GalCer), which had been produced by alkaline deacylation of bovine brain GalCer. Alkaline deacylation maintained the natural *erythro* isomeric form of the sphingoid base in lyso GalCer and avoided racemization to the *threo* form (e.g., Radin, 1990). Thin-layer chromatographic (TLC) analysis using $CHCl_3$/CH_3OH/NH_4OH (6:3:0.5) revealed that the lysoGalCer contained mostly sphingosine (>98%) rather than dihydrosphingosine. After reacylation, *N*-acyl GalSphs were purified by flash column chromatography and recrystallized from −20°C acetone. Traces of silica gel were removed by dissolving the crystallized lipid in hexane/isopropanol (7/2) at 4°C and centrifuging to pellet the silica gel. Lipid purity and *N*-acyl homogeneity were confirmed by TLC and by capillary gas chromatography, respectively, as described by Kulkarni et al. (1995a). $24{:}1^{\Delta 15}$ SO_4-GalCer was synthesized and purified as described previously (Boggs et al., 1988).

Lipid dispersion preparation

Lipid dispersions were prepared in phosphate buffer (pH 6.6) containing 10 mM potassium phosphate, 100 mM sodium chloride, and 1.5 mM sodium azide, following a similar procedure described previously (Kulkarni et al., 1995a,b). Briefly, the vacuum-dried lipid was hydrated with phosphate buffer, incubated above 90°C for 3 min, vortexed vigorously, and briefly bath sonicated (above 90°C). This process was repeated two more times. Then the dispersion was subjected to three freeze-thaw cycles to obtain a uniform distribution of buffer solutes across the bilayers. Rapid freezing was achieved by immersing the lipid suspension in an isopropanol bath cooled by dry ice. During each thawing cycle, the glycolipid dispersion was raised above 90°C and vortexed before subsequent freezing. After the final thawing, the dispersion was equilibrated to room temperature. This procedure did not cause any chemical breakdown of the lipids as assessed by TLC.

Electron microscopy

The procedure for obtaining freeze-fracture replicas remained essentially the same as reported previously (Brown et al., 1995; Kulkarni et al., 1995a,b), except that here we deep-etched the fractured surface to improve microstructure exposure. Briefly, sample aliquots (3 μl) of the lipid dispersions were placed on gold alloy planchets at room temperature (22°C) and then were flash frozen by plunging into liquid propane cooled by liquid nitrogen. To avoid slow-freezing artifacts, liquid propane was used for cryofixation because of its higher cooling rate (19,100°C/s) compared to that of Freon 22 (9,000°C/s) (Sternberg, 1992). No cryoprotectants such as glycerol were mixed with the lipid samples before cryofixation because of the structural changes known to be induced in GalCer samples by glycerol (Brown et al., 1995, and references therein). Using a Balzers BAF-300 freeze-fracture unit, the frozen samples were fractured at −120°C and immediately deep-etched for 6–8 min by warming the stage to −100°C while using the −120°C fracturing knife as a condensing trap. Replicas, produced by

platinum/carbon shadowing at 45° followed by carbon evaporation at 90°, were mounted on 200-mesh copper EM grids and then cleaned using either chloroform/methanol (2/1) mixture or 50% NoChromix in sulfuric acid before being examined in a JEOL 100-S transmission EM. Objects shown in the micrographs are representative of what was observed within a given sample preparation. Reproducibility was checked by preparing and analyzing specimens of identical composition at different times, i.e., different freeze fracture runs.

Negative staining was achieved by applying 2% uranyl acetate solution to grids containing sample and then wicking away the excess after 30–60 s with a filter paper. A detailed description of methodological variations employed to avoid artifacts during negative staining including appropriate controls has been described previously (Kulkarni et al., 1995a).

RESULTS AND DISCUSSION

24:1 GalCer

Fig. 1 shows a typical micrograph of freeze-etched 24:1$^{\Delta 15}$ GalCer prepared by hydration with excess buffered saline followed by cyclic heating and freeze-thawing (see Materials and Methods). Immediately apparent is the nanotubular morphology previously observed after freeze fracture preparation in the absence of deep etching (Kulkarni et al., 1995a,b). Using negative stain EM, Goldstein et al. (1997) recently confirmed that 24:1 GalCer yields nanotubular morphology, but noted that production by the dimethylformamide/water precipitation method resulted in nanotubes somewhat longer (600 nm) and smaller in diameter (13–20 nm) than production by cyclic heating and freeze-thawing in buffered saline (diameters = 25–30 nm). In this regard, it is worth noting that deep etching of 24:1 GalCer, prepared by cyclic heating and freeze-thawing, reveals longer tubules (700–900 nm) than the 250–400-nm lengths depicted by freeze-fracture alone (Kulkarni et al., 1995a,b). Cryo-EM micrographs show such glycolipid tubules to be hollow, with diameters of 20–25 nm (Wilson-Kubalek et al., 1998).

Previously, Mutz et al. (1990) reported that incubation of 24:1 GlcCer in excess water at room temperature resulted in rigid needle-like structures developing from the glycolipid mass and projecting into the aqueous phase, as observed by light microscopy. Warming above the main phase transition temperature of 76°C led to the disappearance of the needles and to the formation of giant membranes. Subsequent cooling transformed the giant membranes into a disorderly array of rigid fibers (Mutz et al., 1990). However, both the diam-

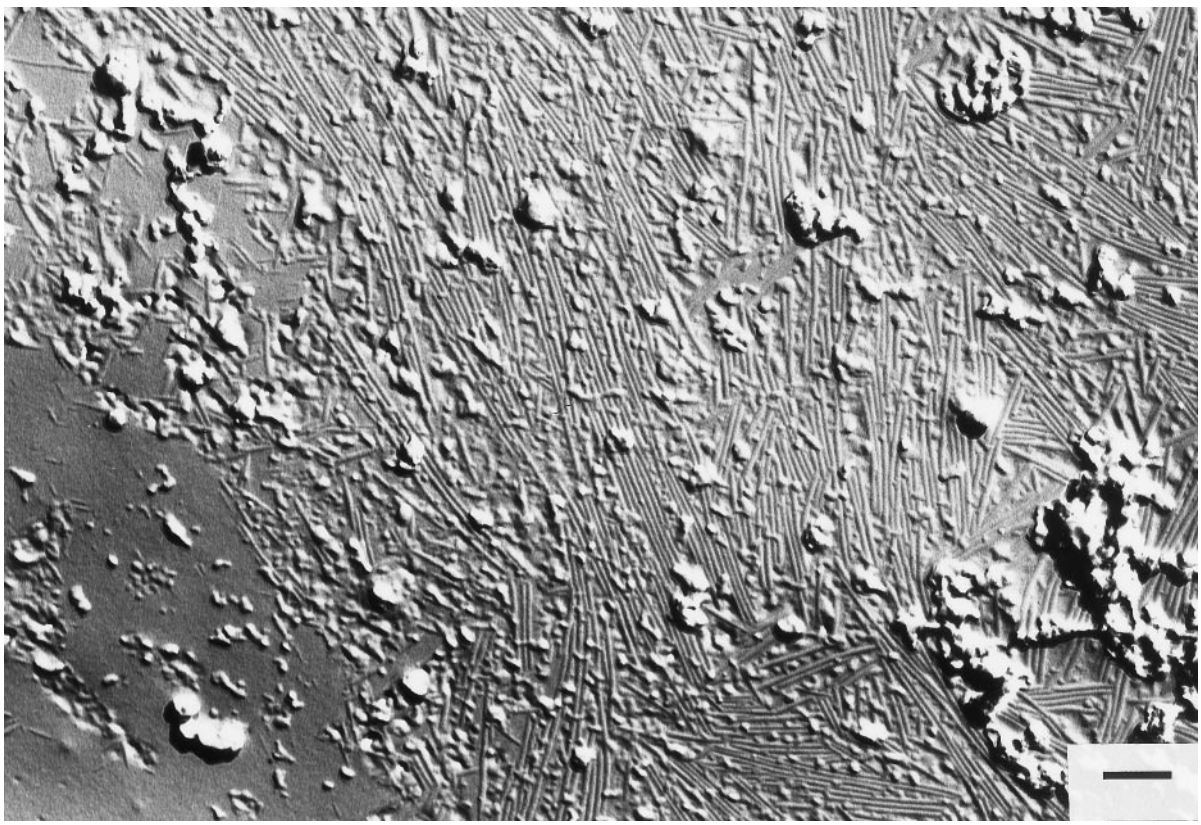

FIGURE 1 Morphology of 24:1$^{\Delta 15}$ GalCer aqueous dispersions. (*A*) Freeze-etch electron micrograph of glycolipid nanotubes. After sample preparation as described in Materials and Methods, aliquots were cryofixed from room temperature (~22°C) by plunging into liquid propane, and platinum/carbon replicas were produced for inspection by transmission electron microscopy. Shadowing direction is from the lower left to the upper right. The bar in the lower right corner represents 250 nm.

eter and length of the 24:1 GlcCer needles and fibers were at least an order of magnitude larger than the dimensions of the 24:1 GalCer nanotubes.

To test various aspects of models developed to explain tubule formation by chiral amphiphiles such as GalCer derivatives, we performed a series of experiments in which the incubation conditions were systematically altered or structural changes were introduced into GalCer itself. Before we report the outcome of these experiments, it is helpful to reiterate the salient features of models describing tubule formation. Helfrich and Prost (1988) first showed that a membrane composed of chiral amphiphiles in a tilted phase will form a cylinder because of an intrinsic bending force due to chirality. The bending force occurs because long chiral molecules do not pack parallel to their neighbors, but rather at a nonzero twist angle. When such neighbors are within a bilayer and are tilted with respect to the local bilayer normal, the favored twist from neighbor to neighbor leads the entire membrane to twist into a cylinder. Over the past decade, the original Helfrich-Prost concept of an intrinsic chiral bending force has been modified and expanded in different ways. The importance of the chiral nature of interaction in driving helix and tubule formation has been emphasized in several subsequent studies (e.g., Yager et al., 1992; Schnur et al., 1994; Zarif et al., 1996; Spector et al., 1996). Selinger et al. (1996) recently reviewed modifications to the original Helfrich-Prost concept, revisited a molecular model for the kinetic formation of lipid tubules by chiral amphiphiles (Schnur et al., 1994), and elaborated an extensive quantitative theory for the equilibrium structure of tubules.

The model describing the putative kinetic process resulting in tubule formation (Fig. 2, *right-side scheme*) can be summarized as follows. When large spherical bilayer vesicles (i.e., flat membranes) are composed of lipids that transform from an untilted to a tilted gel phase upon cooling, tilt order develops based on the chiral packing of the lipid molecules. Tilt order is not uniform throughout the entire bilayer because of the inherent tendency of the molecules to be slightly nonaligned as a result of the chirality of the interaction. The progressive nonalignment of adjacent amphiphiles manifests itself as a linear change in the tilt direction within various stripe-like domains and leads to an inherent cupping or rippling of each stripe-like domain. At the domain walls separating stripes, the tilt direction changes sharply, giving rise to narrow ridges between adjacent stripes. Fragmentation of the stripes is favored along the domain boundaries and can be caused by various defects. Such defects may originate from thermal fluctuations or local differences in response time of sets of molecules to thermal changes. Defects may also be partly due to mechanical disturbances or electrolyte interactions. Because of their inherent tendency to twist, the resulting stripe-like fragments can curl up to form stable tubular-shaped structures from helical ribbons to protect their exposed edges and produce a minimized free energy state. However, helical ribbons can be stable microstructures under certain conditions and need not be intermediate states in the formation of tubules. In fact, our earlier freeze-fracture micrographs of 24:0 GalCer demonstrate the stability of helical ribbons formed by certain glycolipid species (Kulkarni et al., 1995a).

The molecular origin of chirally driven helix formation in amphiphilic assemblies has been addressed in detail by Nandi and Bagchi (1996). They found that the effective pair potential between two chiral molecules depends on the relative sizes of the groups attached to the two chiral centers, on the orientation of the amphiphiles, and on the distance between them. In contrast to mirror-image isomers that align parallel to each other in their minimum energy conformation, a pair of similar enantiomers displays a tilt angle between them, leading to formation of helical morphology. The tilt angle depends not only on the sizes of the groups attached to the chiral centers, but also on elastic forces that can significantly modify the pitch predicted by the chiral interactions alone.

Motivated by the preceding theory of tubule formation and by the model of the kinetic process of tubule formation (Fig. 2, *right side*), we performed the following experiments using 24:1 GalCer. First, to ascertain whether cooling through the main phase transition promoted nanotube formation as suggested by Selinger et al. (1996) and Thomas et al. (1995), we prepared 24:1 GalCer dispersions simply by hydrating the dried glycolipid at room temperature and vortexing for 1–2 min. In the present study, room temperature was 22°C, which is ~45°C below the main enthalpic phase transition temperature of 24:1 GalCer (Kulkarni et al., 1995a; Kulkarni and Brown, 1998). The glycolipid sample was never warmed above its main enthalpic phase transition temperature. Fig. 3 *A* shows that the resulting 24:1 GalCer assemblies were characterized by larger diameter (40–75 nm) folded, shell-like structures occasionally wrapped in a spiral manner. The morphology of these structures differed dramatically from that shown in Fig. 1 and previously (Kulkarni et al., 1995a,b).

Next we determined the effect of a single freeze-thaw cycle in which thawing was performed at room temperature. Once again, the 24:1 GalCer was kept well below its main enthalpic phase transition temperature of 67°C before and during the freeze-thaw cycle. As shown in Fig. 3 *B*, the results indicate a noticeable increase in the formation of small-diameter surface striations and nanotube-like structures. However, large-diameter (120–160 nm), spirally wrapped cochleate structures persisted throughout the mixtures.

Finally, a 24:1 GalCer dispersion was prepared by hydrating the dried glycolipid at elevated temperature (~90°C) for several minutes, followed by vortexing for 1–2 min. Subsequently, the 24:1 GalCer was allowed to cool to room temperature for several hours but was not subjected to freeze-thaw cycles. In representative EM fields (Fig. 3, *C* and *D*), a variety of different microstructures were observed, including a large number of small-diameter nanotubes as well as occasional large-diameter, helically

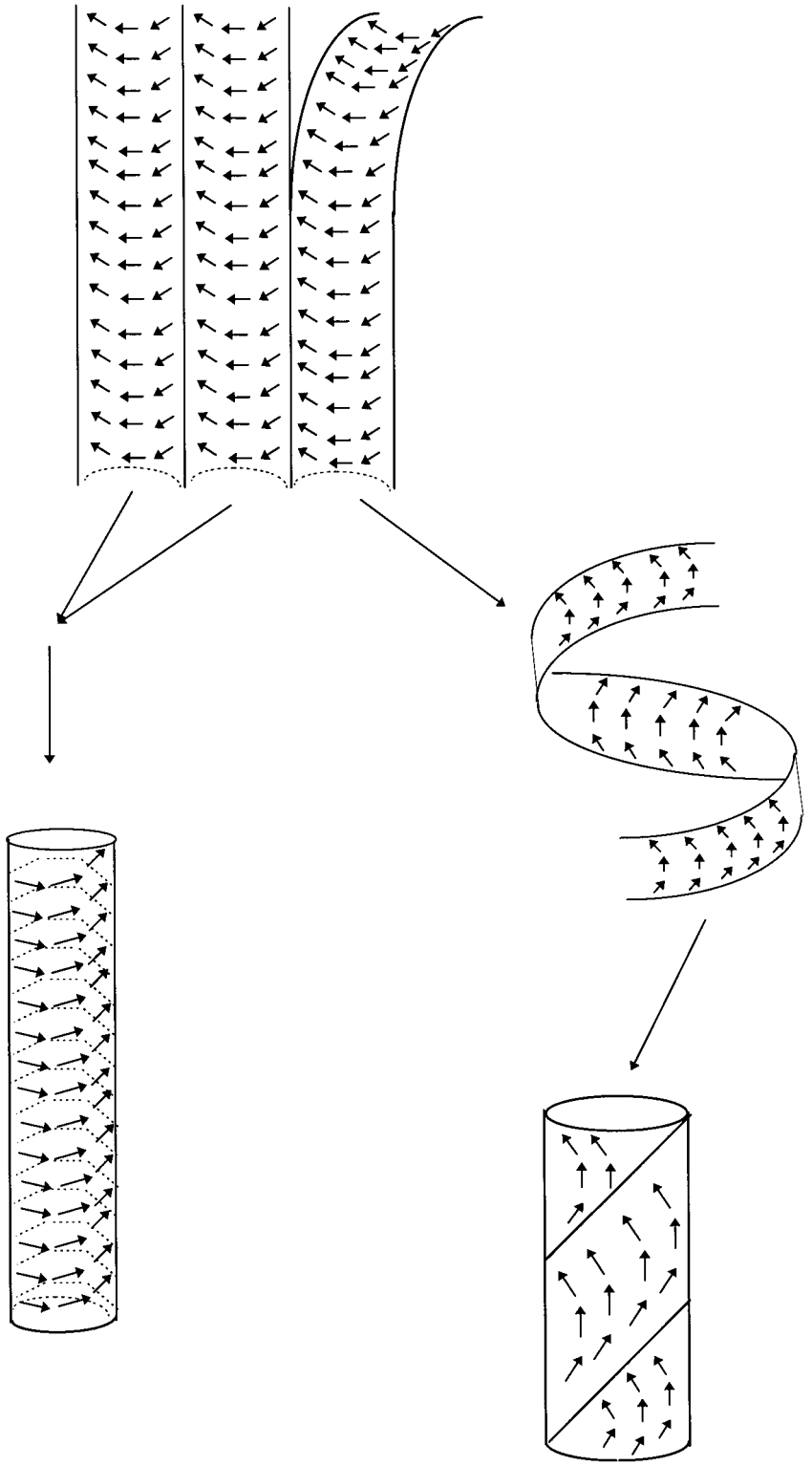

FIGURE 2 Potential modes of nanotube self-assembly. The schematic depicts two potential ways that nanotubes may arise during sample preparation. The representation is a topographic view, and the arrows indicate the tilt direction of different lipid molecules. The mode on the right side depicts a separation of convex-shaped stripe domains along their edge boundaries to yield helically twisted ribbons, which then seal along their edges to form cylindrical tubules, as previously proposed by Schnur et al. (1994). The mode on the left side depicts a nanotube formation mechanism possibly utilized by certain GalCer species (e.g., 22:1 GalCer). In this mechanism, the stripe domains need not pass through a helical ribbon transitional stage before tube formation, but may simply fold over longitudinally and seal into small-diameter nanotubes. More detailed descriptions for both mechanisms are provided in the text.

wrapped cochleate structures and corrugated, fragment-like structures.

Altogether, the preceding results support the important role that cooling through the main phase transition to a gel-like or psuedo-crystalline lipid phase state plays during formation of 24:1 nanotubes, as has previously been predicted (e.g., Thomas et al., 1995; Selinger et al., 1996). In addition, however, freeze-thaw cycling also appears to promote nanotube formation. One plausible explanation is that osmotic forces generated during the freeze-thaw cycling promote fragmentation of the bilayer stripes along the domain boundaries, resulting in tubules of relatively uniform

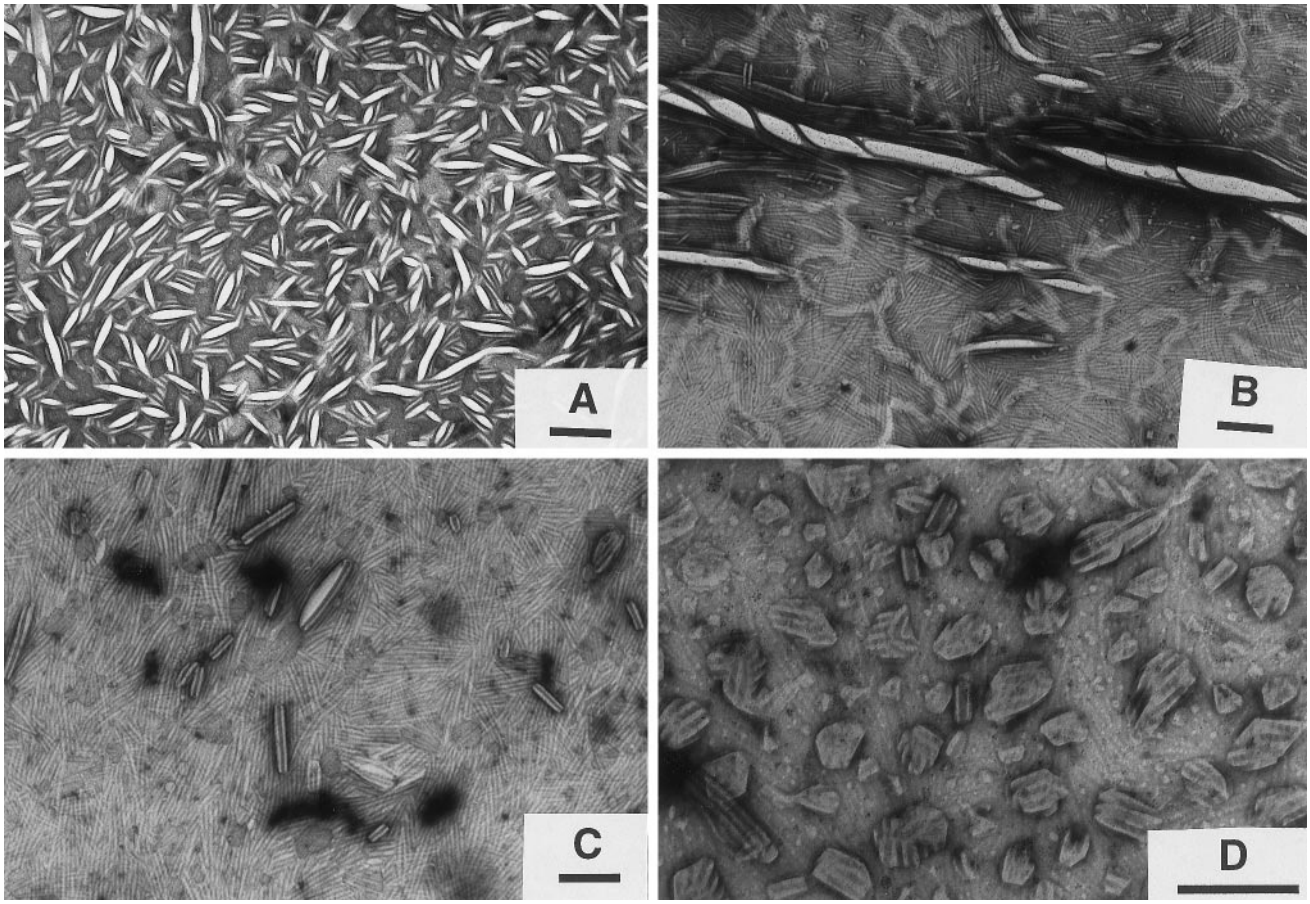

FIGURE 3 Impact of experimental variables on nanotube formation in 24:1$^{\Delta 15}$ GalCer aqueous dispersions. The micrographs for each panel were taken after preparation of 24:1 GalCer by negative stain procedures (see Materials and Methods and Kulkarni et al. (1995a)). The bar in the lower right corner of each panel represents 300 nm. (*A*) 24:1$^{\Delta 15}$ GalCer hydrated by vortexing at room temperature. (*B*) 24:1$^{\Delta 15}$ GalCer hydrated at room temperature and subjected to one freeze-thaw cycle in which thawing was performed at room temperature. (*C* and *D*) 24:1$^{\Delta 15}$ GalCer prepared by hydrating at 90°C, by vortexing followed by cooling to room temperature. No freeze-thaw cycles were used.

diameter. In fact, freeze-thaw processes are well known to generate osmotic forces that fragment and distend membrane bilayers (e.g., MacDonald et al., 1994; Steponkus et al., 1995). MacDonald et al. (1994) noted that multilamellar bilayers composed of certain phosphatidylcholine species appear to be more susceptible than others to fragmenting into small vesicles during freezing and thawing cycles. The fragmentation phenomenon appears to be dependent upon osmotic effects caused by the presence of an electrolyte with a high solubility in water at low temperatures. As noted by MacDonald et al. (1994), the NaCl concentration change that occurs during freezing is ~4.9 osmolal at the eutectic concentration compared to 0.1 osmolal at room temperature for 100 mM NaCl. Under such conditions, a volume reduction approaching 50% in the form of vesicle shrinkage is possible if rupture due to prior internal freezing has not already begun. Hence there is a potential for significant dehydration of lipid polar headgroups during freezing of vesicles in solutions of moderate salt concentrations. The forces caused by such dehydration events are significant and appear to play a major role in the "expansion-induced lysis" of plant cell membranes that are insufficiently acclimated to low temperatures (Steponkus et al., 1995).

Effects of polar headgroup changes on 24:1 glycolipid morphology

In addition to investigating the effects of experimental conditions on nanotube formation by 24:1 GalCer, we also introduced structural changes into GalCer itself by synthetic means to test various aspects of the tubule formation models described earlier.

24:1 SO_4-GalCer

To determine the influence of polar headgroup negative charge on glycolipid morphology, microstructural self-assemblies of *N*-nervonoyl sulfatide, i.e., 24:1 SO_4-GalCer, were studied. Introducing the negatively charged sulfate on the galactose headgroup is known to decrease the average in-plane intermolecular packing density of SO_4-GalCer and to lower the temperature of the major enthalpic phase tran-

sition compared to GalCer (e.g., Boggs et al., 1988; Koynova and Caffrey, 1995). The major enthalpic phase transition temperature of 24:1 SO_4-GalCer is ~20°C lower than that of 24:1 GalCer (Boggs et al., 1988; Kulkarni et al., 1995a; Kulkarni and Brown, 1998). Hence gel phase conditions would be expected from equilibrating 24:1 SO_4-GalCer at room temperature after heating and freeze-thaw cycles. Fig. 4 shows that 24:1 SO_4-GalCer does form large-diameter multilamellar microstructures, but not small-diameter nanotubes. Hence the morphology of 24:1 SO_4-GalCer is strikingly different from the nanotubular appearance of 24:1 GalCer (Fig. 1). The morphology observed in our 24:1 SO_4-GalCer suspensions resembles that of bovine brain sulfatide, which contains substantial amounts of long saturated acyl chains in addition to nervonoyl acyl chains. Archibald and Mann (1994) noted that aqueous suspensions of bovine brain sulfatide form multilamellar vesicles when prepared by vortexing and bath sonicating at 90–100°C for 15 min and then cooling to room temperature. However, if suspended in 100% glycol, heated, and then cooled slowly to room temperature, unilamellar cylinders formed. The lumenal diameter of these unilamellar cylinders reportedly was ~45 nm, and the length ranged from 500 to 700 nm, as revealed by negative stain EM.

24:1 Cer

To determine the effect of removing the galactose polar headgroup on 24:1 glycolipid morphology, 24:1 Cer was equilibrated at room temperature in aqueous buffer and then subjected to a heating and freeze-thaw cycle procedure. As seen in Fig. 5, the resulting 24:1 Cer does form cylindrical bilayer microstructures that are cochleate in nature. Moreover, rather than being only cylindrical in shape, in some cases, the 24:1-Cer microstructures appeared to be cochleate cones. The cochleate appearance of 24:1 Cer cylinders has also been observed by Goldstein et al. (1997).

Effects of acyl chain structural changes on 24:1 glycolipid morphology

In addition to investigating headgroup structural effects, we performed experiments to analyze the impact of changes to acyl structure in GalCer on glycolipid morphological self-assembly. To accomplish this, GalCer derivatives with homogeneous acyl compositions consisting of *cis*-9-octadecenoate ($18:1^{\Delta 9}$), *cis*-11-eicosenoate ($20:1^{\Delta 11}$), or *cis*-13-docosenoate ($22:1^{\Delta 13}$) chains were synthesized and purified as described in Materials and Methods.

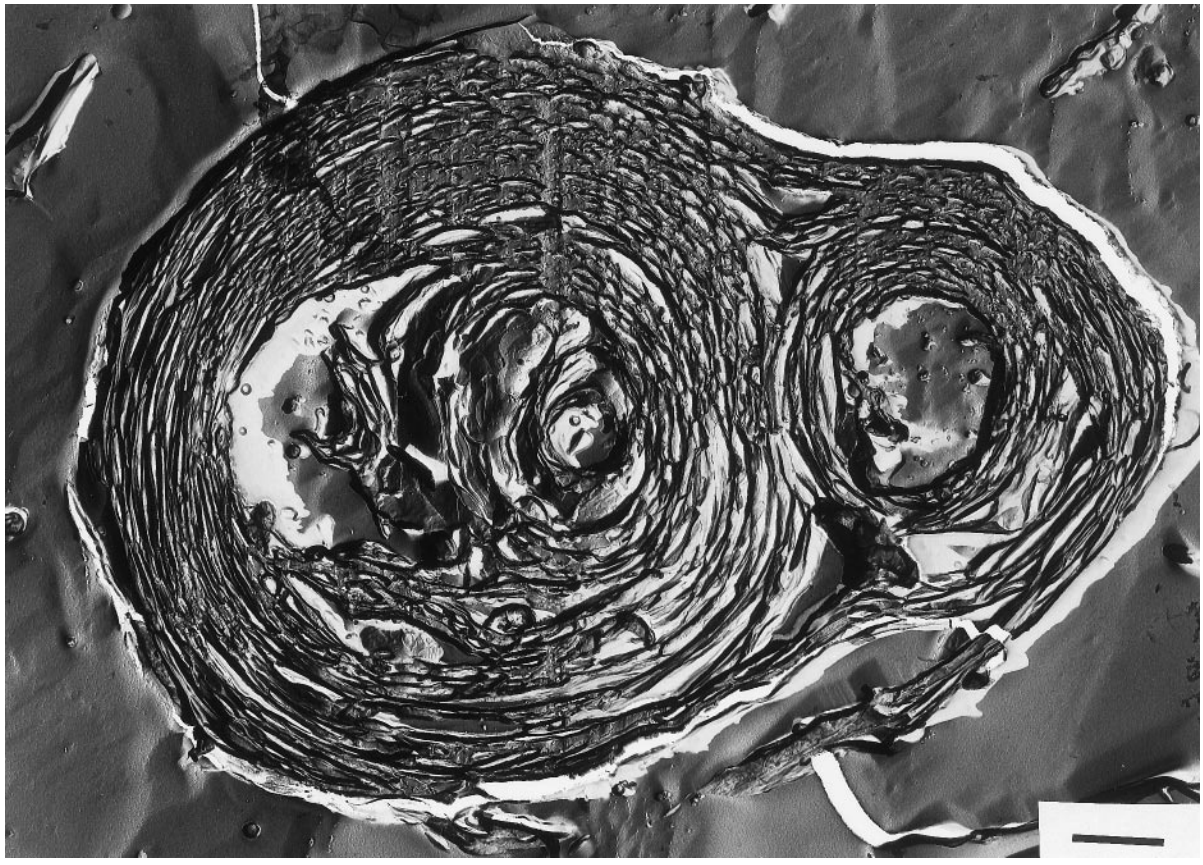

FIGURE 4 Morphology of $24:1^{\Delta 15}$ SO_4-GalCer (sulfatide) aqueous dispersions. Freeze-etch electron micrograph of glycolipid dispersions carried out by cryofixing and producing replicas, as described in Fig. 1. Large-diameter, multilamellar structures predominate. The shadowing direction is from right to left. The bar in the lower right corner represents 1000 nm.

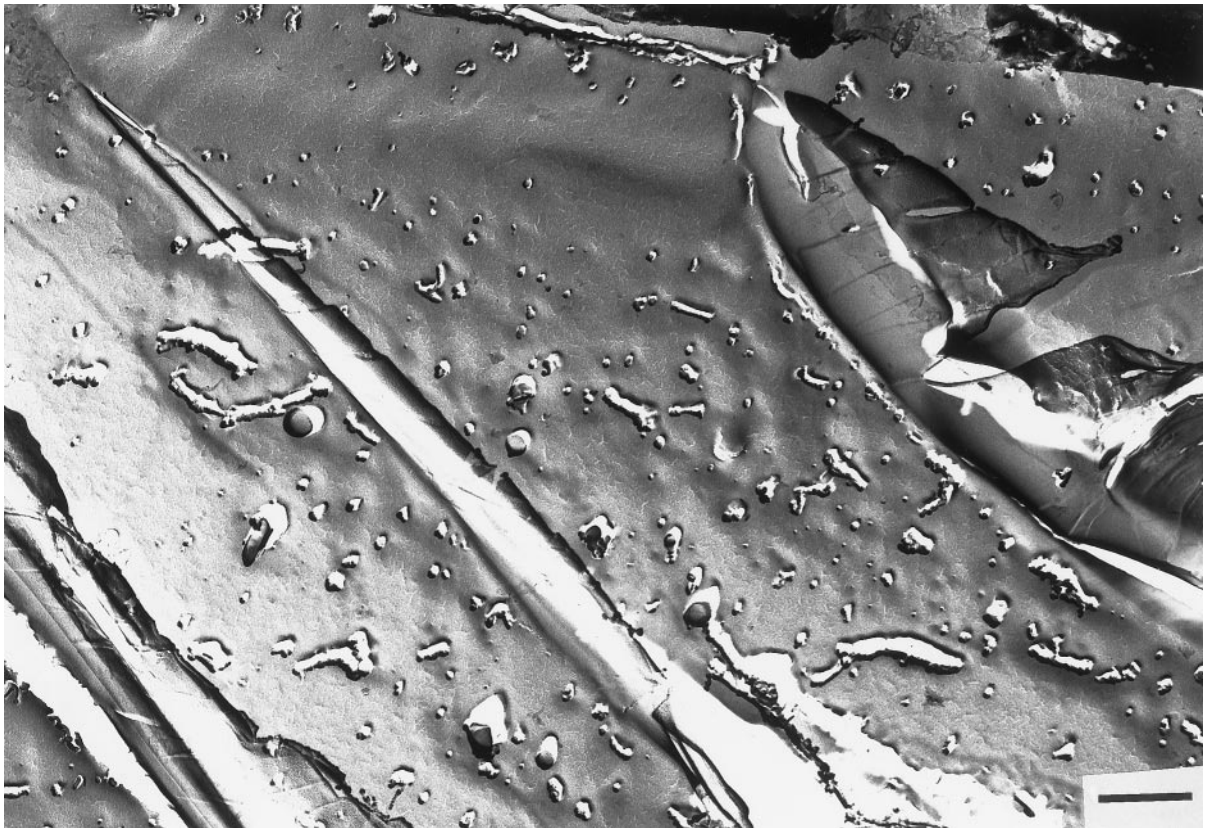

FIGURE 5 Morphology of 24:1$^{\Delta 15}$ Cer aqueous dispersions. Freeze-etch electron micrograph of glycolipid dispersions carried out by cryofixing and producing replicas as described in Fig. 1. The shadowing direction is from the lower left to the upper right. The bar in the lower right corner represents 500 nm.

18:1 GalCer

Multiple types of microstructures, including cochleate cylinders (diameters 80–140 nm), rigid plate-like sheets, as well as giant multilamellar spherical structures, were observed in 18:1$^{\Delta 9(c)}$ GalCer aqueous dispersions (Fig. 6). The variation in morphological form suggests a weakening of the strong, chirally based, nonparallel, intermolecular interactions postulated to occur in titled bilayer phases and thought to drive the entire membrane to twist into a cylinder (Helfrich and Prost, 1988; Selinger et al., 1996). The main enthalpic phase transition of 18:1 GalCer is near 47°C, compared to that of 24:1 GalCer, which is near 67°C (Reed and Shipley, 1989; Kulkarni and Brown, 1998). The 20°C difference in the phase transition temperatures is indicative of weaker intermolecular interactions in 18:1 GalCer compared to 24:1 GalCer. A likely possibility is that the *cis* double bond location between the ninth and tenth carbon atoms near the middle of the acyl chain in 18:1 GalCer provides significant disruptive effects on chain-chain packing. In contrast, the location of the *cis* double bond in 24:1 GalCer is between the 15th and 16th carbon atoms and near the terminal methyl group of the adjacent sphingoid base chain, where the disruptive effects on chain-chain packing will be reduced. The structural basis for these effects has been illustrated previously (Kulkarni and Brown, 1998).

20:1 GalCer and 22:1 GalCer

In earlier studies, 24:0 GalCer was shown to have a main enthalpic phase transition near 82°C (Reed and Shipley, 1987; Gardam and Silvius, 1989; Kulkarni et al., 1995a), to form a partially interdigitated, psuedocrystalline phase (Reed and Shipley, 1987) and to display an undulating ribbon-like morphology (Kulkarni et al., 1995a). As seen in Fig. 7, ribbon-like structures are also observed in 20:1 GalCer. However, the helical ribbons in 20:1 GalCer have right-handed twists. Ribbon widths are 30–35 nm, whereas helical pitches are 80–90 nm. Recent studies of 20:1 GalCer have revealed a main enthalpic phase transition near 61.4°C and have suggested little possibility of transbilayer acyl interdigitation (Kulkarni and Brown, 1998). This situation is in contrast to the behavior of 24:1 GalCer, which has a main enthalpic phase transition near 67°C and probably forms an interdigitated phase upon cyclic heating and freeze/thawing (Kulkarni and Brown, 1998), but which results in bilayer nanotubes (Kulkarni et al., 1995a,b). In this respect, the behavior of 24:1 GalCer is similar to that of 22:1 GalCer, which forms long, nanotube-like cylinders (Fig. 8), has a main enthalpic phase transition near 59°C, and probably forms an interdigitated phase upon cyclic heating and freeze/thawing (Kulkarni and Brown, 1998). The tubules of 22:1$^{\Delta 13(c)}$ GalCer are slightly larger in diameter (35–40 nm)

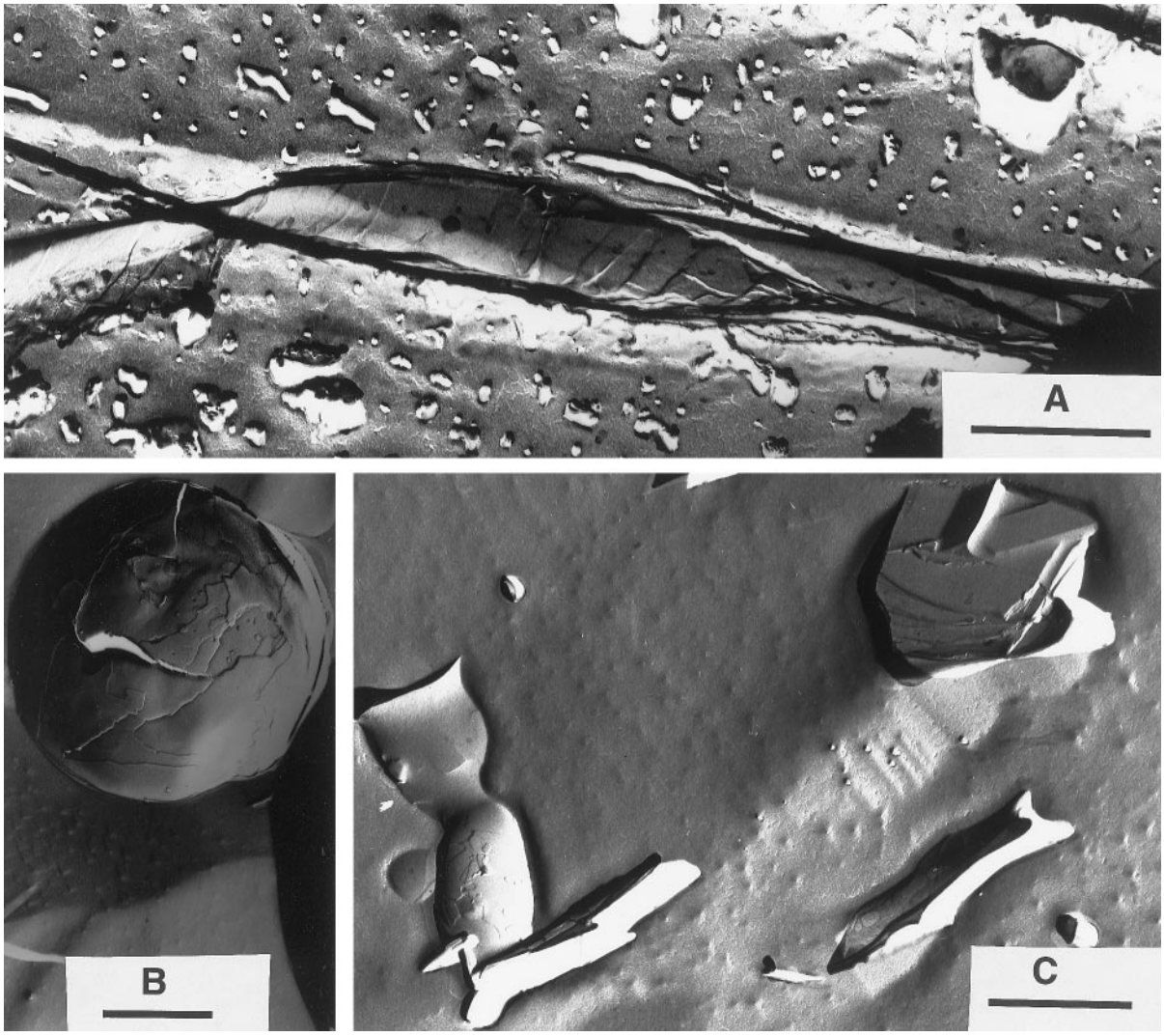

FIGURE 6 Morphology of 18:1$^{\Delta 9}$ GalCer aqueous dispersions. Freeze-etch electron micrograph of glycolipid dispersions carried out by cryofixing and producing replicas as described in Fig. 1. The shadowing direction in *A* is from top to bottom and in *B* and *C* is from the upper left to the lower right. The bars in the lower right corners represent 1000 nm.

than those formed by 24:1$^{\Delta 15(c)}$ GalCer (25–30 nm). The larger diameter and slightly lower enthalpic phase transition temperature suggest a somewhat reduced molecular packing density.

Interestingly, the deep-etch images of 22:1 GalCer appear to show cylindrical tubes emanating from larger arrays that could be due to flattened, adjacently aligned nanotubes or perhaps to a stripe-like phase such as that depicted in the top part of Fig. 2. If due to the latter, the stripe-like appearance may be a visualization of the domain boundaries, where the change in lipid tilt direction gives rise to narrow ridges (or valleys) that separate adjacent stripes. Interestingly, there is no indication that the 22:1 GalCer tubes form as a result of stripe-like ribbons twisting and sealing along their edges, as depicted on the right side of Fig. 2. Rather, the nanotubes appear to emanate directly from the "corduroy-like" surfaces, suggesting the possibility that two or three concave (or convex) stripes might simply self-seal longitudinally to form a tubule upon disruption along the domain walls (Fig. 2, *left*). Careful examination of deep-etched replicas of 24:1 GalCer reveals a similar situation. This raises the possibility that certain GalCer species such as 22:1 GalCer and 24:1 GalCer utilize an alternative mechanism to achieve tubule formation. In contrast, GalCer mixtures containing both 24:0 and 24:1 acyl chains may utilize the single-stripe self-sealing mechanism involving a ribbon intermediate. This would be expected because 24:0 GalCer can form stable ribbons (Kulkarni et al., 1995), whereas 24:1 GalCer forms tubules. The self-sealing ribbon model also has been proposed to explain the formation of the large hollow cylinders (500-nm diameter) by synthetic phospholipids with diacetylenic moieties in their acyl chains (Selinger et al., 1996; Spector et al., 1996, 1997). Obviously, further studies will be required to more fully evaluate these models.

Nonetheless, collectively our results do suggest that the anisotropic chiral interactions thought to be necessary for

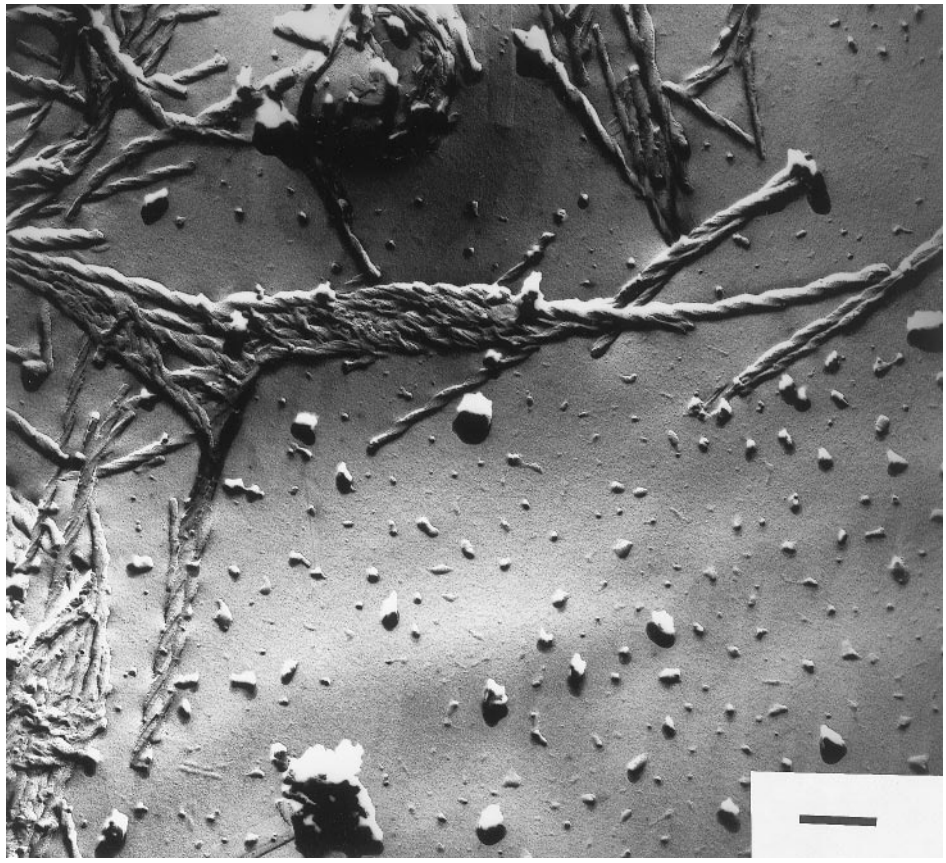

FIGURE 7 Morphology of 20:1$^{\Delta 11}$ GalCer aqueous dispersions. Freeze-etch electron micrograph of glycolipid dispersions carried out by cryofixing and producing replicas as described in Fig. 1. The shadowing direction is from bottom to top. The bar in the lower right corner represents 250 nm.

bilayer nanotube formation are optimal not only when the acyl chain of GalCer is long and monounsaturated, but also when the *cis* double bond location marginally disrupts chain-chain packing. When acyl chain packing is increasingly disrupted by *cis* double bond location (e.g., 18:1 GalCer and 20:1 GalCer), formation of uniform-size tubules appears to be inhibited. Yet when forces controlling acyl chain packing are stronger because of chain saturation as well as the enhanced likelihood of hydrocarbon chain interdigitation (e.g., 24:0 GalCer), ribbon-like structures rather than nanotubes result. Hence an optimum balance of forces controlling the strong, chirally based, nonparallel intermolecular interactions appears to be important in driving segments of the membrane to twist sufficiently to achieve nanotube formation by a self-sealing mechanism involving single stripes (Fig. 2, *right*). In this respect, our experimental observations appear to support several aspects of the theoretical work of Helfrich and Prost (1988), Selinger et al. (1996), and Nandi and Bagchi (1996). Clearly, however, our understanding of the amphiphile structural features that have an impact on nanotube formation is still only at a rather elementary level and will require further investigation.

Being able to predict and control the formation of helical ribbons and tubular microstructures among amphiphiles is important because of their role in various biomedical and biotechnological processes. Intracellular lipid deposits with helical, ribbon-like, and tubular morphologies are known to occur in pathological afflictions such as globoid cell leukodystrophy (Yunis and Lee, 1970), as well as in liver cholestatic disease involving gallstone formation (Chung et al., 1993; Kaplun et al., 1994). On the other hand, lipid assemblies with high axial ratios (i.e., cochleate cylinders and nanotubes) are of interest from a biotechnological perspective because of their potential use as alternative vehicles for controlled and sustained release of drugs, as well as templates during mineralization and metallization microfabrication processes (Schnur, 1993; Archibald and Mann, 1993). Particularly exciting is the recent discovery that glycolipid nanotubes can function as scaffolds that drive protein crystallization processes and result in helically symmetrical arrays for a variety of proteins (Wilson-Kubalek et al., 1998; Darst, 1998). The helical nature of the resulting protein arrays facilitates the acquisition of detailed structural insights and provides a means of obtaining data from relatively small amounts of protein as well as from proteins that are not amenable to crystallization by traditional approaches.

We thank Wayne H. Anderson for assistance with freeze-fracture EM data acquisition during the early stages of this study, and Fred Phillips and Dr. Margot Cleary for their help with the capillary GC analyses of the sphingolipid derivatives.

Portions of this investigation were presented in preliminary form at the FASEB Summer Conference on Molecular Biophysics of Cellular Membranes held at Saxton's River, VT, on July 20–25, 1996, and at the 54th Annual Meeting of the Microscopy Society of America held in Minneapolis, MN, on August 11–15, 1996 (Kulkarni and Brown, 1996).

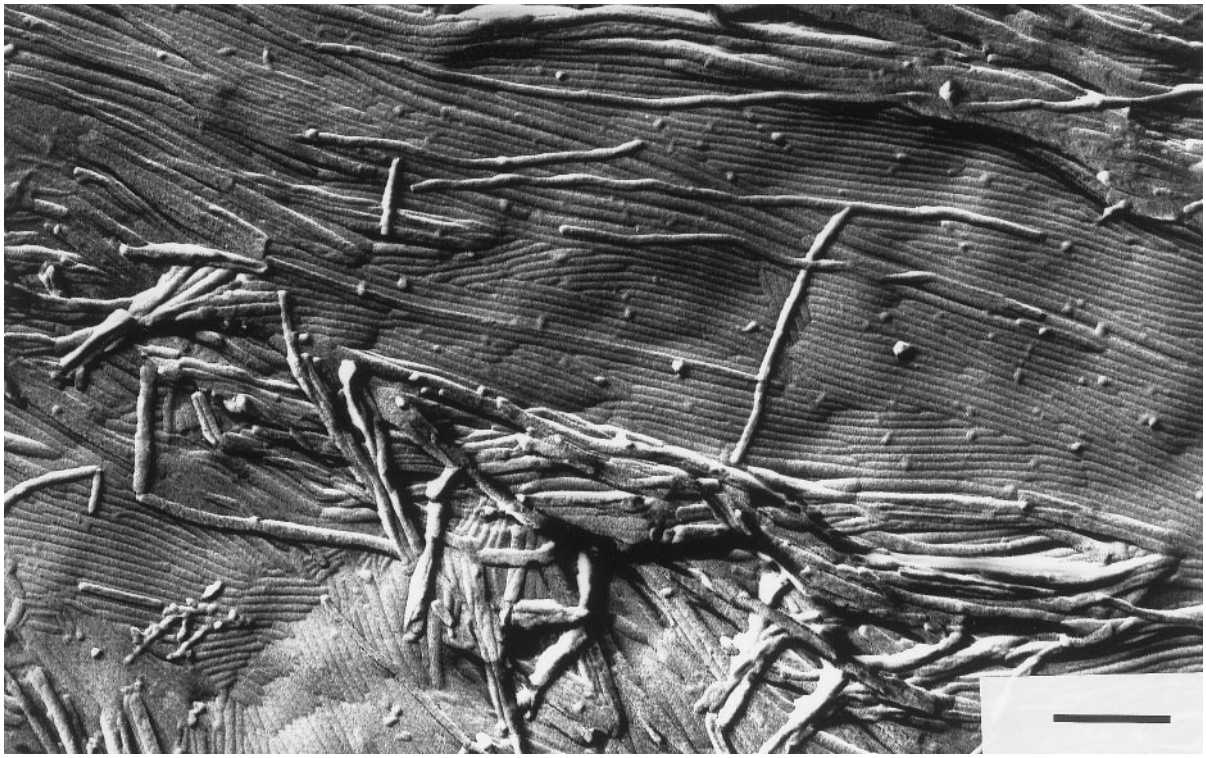

FIGURE 8 Morphology of 22:1$^{\Delta 13}$ GalCer aqueous dispersions. Freeze-etch electron micrograph of glycolipid dispersions carried out by cryofixing and producing replicas as described in Fig. 1. The shadowing direction is from the lower right to the upper left. The bar in the lower right corner represents 250 nm.

The authors gratefully acknowledge the major support provided by U.S. Public Health Service grant GM45928 and the Hormel Foundation.

REFERENCES

Archibald, D. D., and S. Mann. 1993. Template mineralization of self-assembled anisotropic lipid microstructures. *Nature.* 364:430–433.

Archibald, D. D., and S. Mann. 1994. Self-assembled microstructures from 1,2-ethanediol suspensions of pure and binary mixtures of neutral and acidic biological galactosylceramides. *Chem. Phys. Lipids.* 69:51–64.

Archibald, D. D., and P. Yager. 1992. Microstructural polymorphism in bovine brain galactocerebroside and its two major subfractions. *Biochemistry.* 31:9045–9055.

Boggs, J. M., K. M. Koshy, and G. Rangaraj. 1988. Influence of structural modifications on the phase behavior of semi-synthetic cerebroside sulfate. *Biochim. Biophys. Acta.* 938:361–372.

Brown, R. E., W. H. Anderson, and V. S. Kulkarni. 1995. Macro-ripple phase formation in bilayers composed of galactosylceramide and phosphatidylcholine. *Biophys. J.* 68:1396–1405.

Chiu, W., A. J. Avila-Sakar, and M. F. Schmid. 1997. Electron crystallography of macromolecular periodic arrays on phospholipid monolayers. *Adv. Biophys.* 34:161–172.

Chung, D. S., G. B. Benedek, F. M. Konikoff, and J. M. Donovan. 1993. Elastic free energy of anisotropic helical ribbons as metastable intermediates in the crystallization of cholesterol. *Proc. Natl. Acad. Sci. U.S.A.* 90:11341–11345.

Curatolo, W., and L. J. Neuringer. 1986. The effects of cerebrosides on model membrane shape. *J. Biol. Chem.* 261:17177–17182.

Darst, S. A. 1998. A new twist on protein crystallization. *Proc. Natl. Acad. Sci. U.S.A.* 95:7848–7849.

Helfrich, W. 1991. Elastic theory of helical fibers. *Langmuir.* 7:567–568.

Helfrich, W., and J. Prost. 1988. Intrinsic bending force in anisotropic membranes made of chiral molecules. *Phys. Rev. A.* 38:3065–3068.

Gardam, M., and J. R. Silvius. 1989. Intermixing of dipalmitoylphosphatidylcholine with phospho- and sphingolipids bearing highly asymmetric hydrocarbon chains. *Biochim. Biophys. Acta.* 980:319–325.

Goldstein, A. S., A. Lukyanov, P. Carlson, P. Yager, and M. H. Gelb. 1997. Formation of high axial ratio microstructures from natural and synthetic sphingolipids. *Chem. Phys. Lipids.* 88:21–36.

Kaplun, A., Y. Talmon, F. M. Konikoff, M. Rubin, A. Eitan, M. Tadmor, and D. Lichtenberg. 1994. Direct visualization of lipid aggregates in native human bile by light- and cryo-transmission electron-microscopy. *FEBS Lett.* 340:78–82.

Koynova, R., and M. Caffrey. 1995. Phases and phase transitions of the sphingolipids. *Biochim. Biophys. Acta.* 1255:213–236.

Kulkarni, V. S., W. H. Anderson, and R. E. Brown. 1995a. Bilayer nanotubes and helical ribbons formed by hydrated galactosylceramides: acyl chain and headgroup effects. *Biophys. J.* 69:1976–1986.

Kulkarni, V. S., W. H. Anderson, and R. E. Brown. 1995b. Microstructural morphology of sphingolipid dispersions as investigated by freeze-fracture electron microscopy. *In* Proceedings of Microscopy and Microanalysis 1995. G. W. Bailey, M. H. Ellisman, R. A. Hennigar, and N. J. Zaluzed, editors. Jones and Begell Publishing, New York. 944–945.

Kulkarni, V. S., W. H. Anderson, and R. E. Brown. 1995c. Transmission electron microscopy of model biological membranes. *Microsc. Anal.* 1995:19–21.

Kulkarni, V. S., and R. E. Brown. 1996. Modulation of tubular microstructural self-assembly in galactosylceramides: influence of *N*-linked fatty acyl chains. *In* Proceedings of Microscopy and Microanalysis 1996. G. W. Bailey, J. M. Corbett, R. V. W. Dimlich, J. R. Michael, and N. J. Zaluzec, editors. San Francisco Press, San Francisco, CA. 936–937.

Kulkarni, V. S., and R. E. Brown. 1998. Thermotropic behavior of galactosylceramides with *cis*-monoenoic fatty acyl chains. *Biochim. Biophys. Acta.* 1372:347–358.

MacDonald, R. C., F. D. Jones, and R. Qui. 1994. Fragmentation into small vesicles of dioleoylphosphatidylcholine bilayers during freezing and thawing. *Biochim. Biophys. Acta.* 1191:362–370.

Maggio, B., J. Albert, and R. K. Yu. 1988. Thermodynamic-geometric correlations for the morphology of self-assembled structures of glycosphingolipids and their mixtures with dipalmitoylphosphatidylcholine. *Biochim. Biophys. Acta.* 945:145–160.

Mutz, M., R.-M. Servuss, and W. Helfrich. 1990. Giant membranes of swollen phosphatidylethanolamines and glycolipids. *J. Phys. France.* 51:2557–2570.

Nandi, N., and B. Bagchi. 1996. Molecular origin of the intrinsic bending force for helical morphology observed in chiral amphiphilic assemblies: concentration and size dependence. *J. Am. Chem. Soc.* 118: 11208–11216.

Radin, N. S. 1990. Preparative scale isolation of sphingosine. *J. Lipid Res.* 31:2291–2293.

Reed, R. A., and G. G. Shipley. 1987. Structure and metastability of *N*-lignocerylgalactosylsphingosine (cerebroside) bilayers. *Biochim. Biophys. Acta.* 896:153–164.

Reed, R. A., and G. G. Shipley. 1989. Effect of chain unsaturation on the structure and thermodynamic properties of galactocerebrosides. *Biophys. J.* 55:281–292.

Schnur, J. M. 1993. Lipid tubules: a paradigm for molecularly engineered structures. *Science.* 262:1669–1676.

Schnur, J. M., B. R. Ratna, J. V. Selinger, A. Singh, B. Jyothi, and K. R. K. Easwaran. 1994. Diacetylenic lipid tubules: experimental evidence for a chiral molecular architecture. *Science.* 264:945–947.

Selinger, J. V., F. C. MacKintosh, and J. M. Schnur. 1996. Theory of cylindrical tubules and helical ribbons of chiral lipid membranes. *Phys. Rev. E.* 53:3804–3818.

Smaby, J. M., V. S. Kulkarni, M. Momsen, and R. E. Brown. 1996. The interfacial elastic packing interactions of galactosylceramides, sphingomyelins, and phosphatidylcholines. *Biophys. J.* 70:868–877.

Spector, M., K. Easwaran, G. Jyothi, J. Selinger, A. Singh, and J. Schnur. 1996. Chiral molecular self-assembly of phospholipid tubules: a circular dichroism study. *Proc. Natl. Acad. Sci. U.S.A.* 93:12943–12946.

Spector, M., J. V. Selinger, and J. M. Schnur. 1997. Thermodynamics of phospholipid tubules in alcohol/water solutions. *J. Am. Chem. Soc.* 119:8533–8539.

Steponkus, P. L., M. Uemura, and M. S. Webb. 1995. Freeze-induced destabilization of cellular membranes and lipid bilayers. *In* Permeability and Stability of Lipid Bilayers. E. A. Disalvo and S. A. Simon, editors. CRC Press, Boca Raton, FL. 77–104.

Sternberg, B. 1992. Freeze-fracture electron microscopy of liposomes. *In* Liposome Technology, Vol. 1, 2nd Ed. G. Gregoridadis, editor. CRC Press, Boca Raton, FL. 363–383.

Thomas, B. N., C. R. Safinya, R. J. Plano, and N. A. Clark. 1995. Lipid tubule self-assembly: length dependence on cooling rate through a first-order phase transition. *Science.* 267:1635–1637.

Wilson-Kubalek, E., H. Celia, R. E. Brown, and R. A. Milligan. 1998. Lipid nanotubes as substrates for helical crystallization of macromolecules. *Proc. Natl. Acad. Sci. U.S.A.* 95:8040–8045.

Yager, P., J. Chappell, and D. D. Archibald. 1992. When lipid bilayers won't form liposomes: tubules, helices, and cochleate cylinders. *In* Biomembrane Structure and Function—The State of the Art. B. P. Gaber and K. R. K. Easwaran, editors. Adenine Press, Schenectady, NY. 1–18.

Yunis, E. J., and R. E. Lee. 1970. Tubules of globoid leukodystrophy: a right-handed helix. *Science.* 169:64–66.

Zarif, L., A. Polidori, B. Pucci, T. Gulik-Krzywicki, A. A. Pavia, and J. G. Reiss. 1996. Effect of chirality on the formation of tubules from glycolipidic amphiphiles. *Chem. Phys. Lipids.* 79:165–170.